Fernández-Sáez, J. … et al. (2019). Transverse free vibration of resonant nanoplate mass sensors: Identification of an attached point mass. *International Journal of Mechanical Sciences*, v. 150, pp.: 217-225.

DOI: https://doi.org/10.1016/j.ijmecsci.2018.09.055

Transverse free vibration of resonant nanoplate mass sensors: identification of an attached point mass

J. Fernández-Sáez[a], A. Morassi[b], L. Rubio[c], R. Zaera[a,*]

[a] *Department of Continuum Mechanics and Structural Analysis, Universidad Carlos III de Madrid, Av. de la Universidad 30, 28911 Leganés, Madrid, Spain*
[b] *Polytechnic Department of Engineering and Architecture, University of Udine, via Cotonificio 114, 33100 Udine, Italy*
[c] *Department of Mechanical Engineering, Universidad Carlos III de Madrid, Av. de la Universidad 30, 28911 Leganés, Madrid, Spain*

Abstract

In this paper we analyze for the first time the bending vibration of a nanoplate with an attached mass using the strain gradient elasticity theory for homogeneous Lamé material, under Kirchhoff-Love's kinematical assumptions. The exact eigenvalues of the nanoplate vibrating with an attached mass are obtained for a general case, and an approximate closed form expression is provided if the intensity of the mass is small with respect to the total mass of the nanoplate. The inverse problem of identifying a point mass attached on a simply supported rectangular nanoplate from a selected minimal set of resonant frequency data is also considered. We show that if the point mass is small, then the position of the point mass and mass size can be determined by means of closed form expressions in terms of the changes induced by the point mass on the first three resonant frequencies. The identification procedure has been tested on an extended series of numerical simulations, varying the scale parameter of the nanoplate's material and the position and size of the point mass.

Keywords: Strain gradient theory, nanoplates with attached mass,

*Corresponding author. E-mail address: ramon.zaera@uc3m.es

nanosensors, transverse vibration, mass identification, inverse problems.

1. Introduction

Nanosensors are gathering attention in the last years due to the necessity of measuring physical and chemical properties in industrial or biological systems in the submicron scale. In the last decade, the improvement in manufacturing techniques gave rise to a size reduction of nano-electro-mechanical systems (NEMS), resulting in remarkable advances in fabrication costs, power consumption and integration. The reduced dimensions of these transducers lead to novel sensing concepts and to an enhanced performance with a great impact on a diversity of applications [1, 2].

One of the most representative examples of the advantages of downscaling in sensoring systems is the nanomechanical resonator, which consists in a vibrating structure (nanowire, nanocantilever, nanoplate) with remarkable perfomance in detecting small adherent masses which produce slight changes in the resonant frequencies of the system [3]. These label-free sensors show high sensitivity and measurement precission for several reasons: low mass, high quality factor, and high signal-to-noise ratios. Miniaturization of these resonators has moved the resolution of mass detection from the picogram to the zeptogram range in less than a decade [4].

Derived from atomic force microscopy techniques, the nanocantilever-based sensor is the most common structural typology used for mass detection. The benefits of these types of sensors rely on their tiny work area, low fabrication cost, simple integration with electronics, and the possibility to fabricate arrays of tens to thousands of cantilever beams [5]. From its beginnings, cantilevers have been used for the detection of micro-sized particles [6], cells and fungal spores

[7, 8], DNA molecules [9], and even atoms [10, 11]. Up to now, nanocantilevers are still the major player in sensing applications [1].

Although less prevalent than cantilevers, some recent studies have investigated the suitability of 2D resonators for sensing uses. Membranes and plates show, with respect to cantilevers, a much higher quality factor (Q-factor) in fluid media, thus having better signal-to-noise ratio and resolution and making them a great candidate for the development of in-situ biosensors [12, 13, 14, 15]. Moreover, plates are stiffer than cantilevers of the same mechanical properties and length similar to that of the edges of the plate, which increases robustness as a relevant feature for manufacturing and functionalization, as well as mass sensitivity [16]. Nanoplate resonating structures with high Q-factor in air and prominent mass sensitivity have been fabricated by Bhaswara et al. [16].

A key feature of the nanostructures is the need of considering size effects when modeling its mechanical response, since their dimensions become comparable to the characteristic microstructural distances. To that aim, molecular dynamic formulations have been used but these are time consuming, and require the definition of complex interaction potentials. Thus, continuum approaches present advantages in terms of computational cost. Classical –scale free– continuum solid mechanics theories may fail when the characteristic lengths of the studied phenomena are comparable to the size of microstructure. In contrast, generalized continuum models succeed in capturing the effects of microstructure and size effects [17, 18, 19, 20, 21, 22].

Later on, Eringen postulated [23, 24] an integral nonlocal constitutive relation for microstructured materials. From this earlier nonlocal theories, he derived a differential version [25]. This model has been widely used to address problems related to different kind of structural elements (see the recent reviews by Eltaher et al. [26], and Rafii-Tabar et al. [27] on this last topic). However, some paradoxical results derived from the nonlocal model have been found both in static [28] and dynamic [29] conditions. Romano et al. [30] recenty shown

that, in the majorities of the cases, the integral formulation of the fully nonlocal elasticity theory leads to problems that have to be considered as ill-posed, having no solution in general. Thus, previous attempts to overcome the quoted paradoxical results [31, 32] have proven to be inadequate, all of this putting the focus on other generalized continuum theories, such as mixed local/nonlocal [33, 34] or gradient formulations.

The development of efficient methods for the identification of concentrated masses in nanostructures is essential for their use as sensors. Particularly, for nanoplates and graphene sheets, techniques have been recently proposed by different authors [35, 36, 37, 38, 39, 40, 41]. However, the above developments are based on the Eringen fully nonlocal theory that, as stated above, leads to ill-posed problems [30]. Thus, alternative theories have to be considered for the proposal of identification methods in 2D nanosensors.

Among the different strain gradient theories, the one proposed by Lam et al. [42] has been used by different authors to model the mechanical behaviour of nanostructures. Known as the modified strain gradient elasticity theory, this model is based on previous developments by Mindlin [22] and Fleck and Hutchinson [43]. The application of the principle of virtual work (see Germain [44], for instance) leads to additional balance equations, and the number of length-scale parameters is reduced from five (in the original model by Mindlin for isotropic center-symmetric materials) to three. The modified strain gradient theory has been used for the analysis of static and vibrational behaviour of Euler-Bernoulli beams [45], Timoshenko beams [46], and Kirchhoff plates [47], as well as for the study of buckling behaviour of Euler-Bernoulli beams [48] and shear deformable beams [49]. Recently, Zhang et al. [50] applied this theory to model the static bending, buckling and free vibration of a size-dependent Kirchhoff micro-plate resting on elastic medium. Likewise, Morassi et al. [51] analyzed the axial vibrational behaviour of a nanorod carrying a concentrated mass through its span using the modified strain gradient theory. Moreover, for

the case of small intensity of the concentrated mass, a first order perturbative technique was derived to compute the natural frequencies of the nanorod. In fact, from the properties of the eigenvalue perturbative theory, the identification of a single point mass in a uniform nanorod (mass intensity and position) by minimal frequency data can be performed. Later on, Dilena et al. [52] extended this analysis to describe the bending behaviour of a nanoresonator modelled as a Euler-Bernoulli beam carrying a single point mass, likewise using the modified strain gradient theory, and developed a method for the identification of the point mass from minimal eigenfrequency data.

In this paper we obtain the natural frequencies for the bending vibration of a nanoplate with an attached mass within the modified strain gradient constitutive framework [42]. To that aim we use the corresponding model proposed by Wang et al. [47] for the Kirchhoff plate behaviour, accounting for lenght-scale effects. Moreover we also consider the inverse problem of determining the intensity and position of a point mass attached to a simply supported rectangular nanoplate from minimal natural frequency data. For the case of small intensity of the concentrated mass, and adopting the approach derived by Rubio et al. [53] for plates following classical elasticity, we show that the inverse problem can be formulated and solved in closed form in terms of the changes induced by the point-mass on the first three natural frequencies. The novelty of the article lies in the analysis of the bending vibration of a nanoplate with an attached mass using the modified strain gradient theory. To the best of our knowledge, both the study of the direct problem and the inverse problem are addressed here for the first time. Moreover, even the key mathematical tool for formulating and solving the inverse problem, namely the explicit expression of the sensitivity of the resonant frequencies to the point mass, see equation (44), is a relevant element of originality of the present work that had not previously appeared in the literature.

The paper is organized as follows. The problem of the free bending vibration

of the nanoplate is presented in section 2, while sections 3 and 4 are devoted to the analysis of the effect of the presence of an attached point mass. In section 3 the exact natural frequencies are obtained, and in section 4 an approximate solution for the eigenvalues of the nanoplate are derived, provided that the intensity of the point mass is small. Section 5 addresses the inverse problem of identifying the intensity and position of the small point mass from eigenfrequency shifts. Section 6 reports and discusses the results of numerical simulations, both of the direct and the inverse eigenvalue problem. Section 7 presents the concluding remarks of this work.

2. Modified strain gradient model for the bending vibration of a nanoplate

The modified strain gradient theory was presented by Lam et al. [42] as a simplification of a previous formulation by Mindlin [22]. The application of the principle of virtual work (see Germain [44], for instance) to this approach leads to additional balance equations related to the higher-order stress and strain gradients considered, and for isotropic materials contains three non-classical material parameters in addition to the conventional Lame moduli. Brief resumes of the theory can be found in papers by Kong et al. [45], Akgoz and Civalek [48], Morassi et al. [51] and Wang et al. [47], among others.

Based in the cited theory, let us formulate the transverse free vibration problem for a simply supported nanoplate with rectangular mid-plane $\Omega = \{(x, y) \in \mathbb{R}^2 | 0 < x < a, 0 < y < b\}$ and equivalent uniform thickness $h > 0$. Assuming the kinematic hypothesis of Kirchhoff-Love's plate theory, the equation governing the transverse displacement $U(x, y, t)$ of the nanoplate reads as, see [47] for details,

$$\rho \ddot{U}(x, y, t) - p_1 \triangle^3 U(x, y, t) + p_2 \triangle^2 U(x, y, t) = 0, \tag{1}$$

where $\ddot{U}(x, y, t)$ indicates the second partial derivative of U with respect to t,

$t > 0$, and $\triangle$ is the Laplacian operator, e.g., $\triangle \equiv \frac{\partial^2}{\partial x^2} + \frac{\partial^2}{\partial y^2}$.

In the above equation, the surface mass density is denoted by $\rho = \gamma h$ (γ is the volume mass density), and the quantities p_1, p_2 are given by

$$p_1 = \mu I(2\ell_0^2 + \frac{4}{5}\ell_1^2), \tag{2}$$

$$p_2 = \mu h(2\ell_0^2 + \frac{8}{15}\ell_1^2 + \ell_2^2) + \frac{E}{1-\sigma^2} I, \tag{3}$$

where $I = \frac{h^3}{12}$, $\mu > 0$ is the elastic shear modulus, $E > 0$ is the Young's modulus, σ is the Poisson's coefficient of the material, and the scale parameters are denoted by ℓ_0, ℓ_1, ℓ_2.

Using the classical separation of variables method, the transverse displacement of the nanoplate $U(x, y, t)$ can be expressed as

$$U(x, y, t) = u(x, y) \exp i\omega t, \tag{4}$$

$u(x, y)$ being the amplitude of the normal vibration mode (eigenfunction) associated to the natural (radian) frequency of the motion ω, and i is the imaginary unit. Therefore, from (1) and (4), the free undamped infinitesimal transverse vibration $u = u(x, y)$ of the nanoplate consists in finding $u \in H^6(\Omega) \setminus \{0\}$, $\lambda \in \mathbb{R}^+$, solution to

$$\begin{cases} L[u] \equiv p_2 \Delta^2 u - p_1 \Delta^3 u = \lambda \rho u, \quad \text{in } \Omega, & (5) \\ u = 0, \quad \text{on } \partial\Omega, & (6) \\ u_{,\nu\nu} = 0, \quad \text{on } \partial\Omega, & (7) \\ P_1 u_{,\nu\nu} - P_4 u_{,\nu\nu\nu\nu} = 0, \quad \text{on } \partial\Omega, & (8) \end{cases}$$

where $\lambda = \omega^2$ and ν is the unit outer normal to $\partial\Omega$. Hereinafter, for m integer and $m \geq 1$, $H^m(\Omega)$ denotes the usual Sobolev space of Lebesgue measurable functions $f : \Omega \to \mathbb{R}$ with square-summable weak derivative $D^\alpha f$ up to the order m, e.g., $H^m(\Omega) = \{f : \Omega \to \mathbb{R} | \ \int_\Omega |f|^2 + \sum_{|\alpha|=1}^m |D^\alpha f|^2 < +\infty\}$, where

$\alpha = (\alpha_1, ..., \alpha_n)$, $\alpha_i \geq 0$ integer, $|\alpha| = \alpha_1 + ... + \alpha_n$, $D_i = \frac{\partial}{\partial x_i}$, $D^\alpha = D_1^{\alpha_1} ... D_n^{\alpha_n}$, $n = 2$.

The classical, (6) and (7), and nonclassical, (8), boundary conditions correspond to a simply supported nanoplate [47]. The coefficients appearing on the boundary conditions (8) are given by

$$P_1 = c_1 h + c_2 I, \tag{9}$$

$$P_4 = c_7 I, \tag{10}$$

with

$$c_1 = \mu(2\ell_0^2 + \frac{8}{15}\ell_1^2 + \ell_2^2), \tag{11}$$

$$c_2 = \frac{E}{1-\sigma^2}, \tag{12}$$

$$c_7 = p_1/I. \tag{13}$$

To find the weak formulation of the problem (5)–(8), let us introduce the set of admissible deformations $\mathcal{H}$:

$$\mathcal{H} = \{\varphi : \Omega \to \mathbb{R} |\ \varphi \in H^3(\Omega),\ \varphi = \varphi_{,\nu\nu} = 0 \text{ on } \partial\Omega\}. \tag{14}$$

Multiplying (5) by any $\varphi \in \mathcal{H}$, we obtain

$$(L[u], \varphi) = \int_\Omega p_2(\Delta^2 u)\varphi - \int_\Omega p_1(\Delta^3 u)\varphi \equiv (L_2[u], \varphi) - (L_1[u], \varphi). \tag{15}$$

Let us consider $(L_2[u], \varphi)$. Integrating by parts twice, recalling that $\varphi = 0$ on $\partial\Omega$ and observing that (by (6) and (7)) $\Delta u = 0$ on $\partial\Omega$, we have

$$(L_2[u], \varphi) = \int_\Omega p_2 \Delta u \Delta\varphi. \tag{16}$$

Analogous calculations can be repeated for the second term of (15), obtaining

$$(L_1[u], \varphi) = -\int_{\partial\Omega} p_1(\Delta^2 u)\nabla\varphi \cdot \nu + \int_\Omega (\Delta^2 u)\Delta\varphi, \tag{17}$$

where $\cdot$ denotes the scalar product in $\mathbb{R}^2$. Now, from (6), (7) and (8), we have $\Delta^2 u = 0$ on $\partial\Omega$ and the first term in (17) vanishes. Integrating by parts once again, and observing that, by definition, $\Delta\varphi = 0$ on $\partial\Omega$, we have

$$(L_1[u], \varphi) = -\int_\Omega p_1 \nabla(\Delta u) \cdot \nabla(\Delta\varphi). \tag{18}$$

Therefore, inserting (16) and (18) in (15), we obtain that, if $(u \in H^6(\Omega)\setminus\{0\}, \lambda)$ is an eigenpair to (5)–(8), then (u, λ) is also a solution of the weak formulation of the eigenvalue problem: to determine $(u \in H^3(\Omega) \setminus \{0\}, \lambda)$ such that

$$\int_\Omega p_2 \Delta u \Delta\varphi + p_1 \nabla(\Delta u) \cdot \nabla(\Delta\varphi) = \lambda \int_\Omega \rho u \varphi, \quad \text{for every } \varphi \in \mathcal{H}. \tag{19}$$

Conversely, it is possible to prove that if (u, λ) is an eigensolution to (19), and $u \in H^6(\Omega)$, then (u, λ) solves also (5)–(8), and the equivalence between the strong and the weak formulation is proved.

We now determine the eigensolutions to (5)–(8). By direct inspection, the pairs

$$\lambda_{mn} = \frac{1}{\rho}\left(\mathcal{C}_1(m,n)p_1 + \mathcal{C}_2(m,n)p_2\right), \tag{20}$$

$$u_{mn}(x,y) = \sqrt{\frac{4}{\rho a b}} \sin\left(\frac{m\pi x}{a}\right) \sin\left(\frac{n\pi y}{b}\right), \tag{21}$$

$m = 1, 2, ...,$ $n = 1, 2...,$ are eigensolutions to (5)–(8), with

$$\mathcal{C}_1(m,n) = \left(\left(\frac{m\pi}{a}\right)^2 + \left(\frac{n\pi}{b}\right)^2\right)^3, \tag{22}$$

$$\mathcal{C}_2(m,n) = \left(\left(\frac{m\pi}{a}\right)^2 + \left(\frac{n\pi}{b}\right)^2\right)^2. \tag{23}$$

Actually, it is possible to prove that (20), (21) are all the possible eigensolutions to (5)–(8). To see this, let us proceed by contradiction and assume there exists another eigenfunction v, $v \in H^6(\Omega) \setminus \{0\}$, associated to the eigenvalue λ, with $\lambda \neq \lambda_{mn}$ for every $m, n = 1, 2, ...$ By writing the weak formulation (19) for the eigenpairs (u_{mn}, λ_{mn}) and (v, λ), and subtracting term by term, we have

$$\int_\Omega \rho v u_{mn} = 0, \quad \text{for every } m, n \geq 1. \tag{24}$$

Since $\{u_{mn}\}_{m,n=1}^{\infty}$ is a complete family in $L^2(\Omega)$, from (24) we have $v \equiv 0$ in Ω, which is a contradiction.

3. Free transverse vibration of a nanoplate with an attached point mass

In this section we shall assume that a point mass M is attached to the plate at the point $P_0 = (x_0, y_0) \in \Omega$. The strong formulation of the eigenvalue problem, analogous to (5)–(8), is

$$\begin{cases} L[\widetilde{u}] = \widetilde{\lambda}(\rho + M\delta_{P_0})\widetilde{u}, \quad \text{in } \Omega, & (25) \\ \widetilde{u} = 0, \quad \text{on } \partial\Omega, & (26) \\ \widetilde{u}_{,\nu\nu} = 0, \quad \text{on } \partial\Omega, & (27) \\ P_1\widetilde{u}_{,\nu\nu} - P_4\widetilde{u}_{,\nu\nu\nu\nu} = 0, \quad \text{on } \partial\Omega, & (28) \end{cases}$$

where $(\widetilde{u}, \widetilde{\lambda})$ is the eigenpair, $\widetilde{u} \in H^6(\Omega \setminus \{P_0\}) \cap H^2(\Omega) \setminus \{0\}$, $\widetilde{\lambda} \in \mathbb{R}$ and δ_{P_0} denotes the Dirac's delta with support at $P_0 \in \Omega$. The weak formulation of (25)–(28) consists in determining $(\widetilde{u} \in H^3(\Omega \setminus \{P_0\}) \cap H^2(\Omega) \setminus \{0\}, \widetilde{\lambda} \in \mathbb{R})$ such that

$$\int_\Omega p_2 \Delta\widetilde{u}\Delta\varphi + p_1 \nabla(\Delta\widetilde{u})\cdot\nabla(\Delta\varphi) = \lambda\left(M\widetilde{u}(P_0)\varphi(P_0) + \int_\Omega \rho\widetilde{u}\varphi\right), \text{ for every } \varphi \in \mathcal{H}. \tag{29}$$

The eigenpairs of (25)–(28) or, equivalently, of (29) do not have explicit closed form as in the case $M = 0$. However, we can provide an explicit expression for the frequency equation of the supported nanoplate with a point mass M at P_0. Let us rewrite (25) as

$$L[\widetilde{u}] - \widetilde{\lambda}\rho\widetilde{u} = f, \quad \text{in } \Omega, \tag{30}$$

with

$$f = \widetilde{\lambda}M\delta_{P_0}\widetilde{u}, \tag{31}$$

and define

$$\widetilde{u}(x, y) = \sum_{m,n=1}^{\infty} c_{mn} \sin\left(\frac{m\pi x}{a}\right) \sin\left(\frac{n\pi y}{b}\right), \tag{32}$$

where the series is assumed to be uniformly convergent in Ω together with high order partial derivatives. Replacing (32) in (30), multiplying by $\sin\left(\frac{k\pi x}{a}\right)\sin\left(\frac{j\pi y}{b}\right)$, with $k,\ j,\ k,j \geq 1$, and integrating in Ω, we obtain

$$c_{mn} = \frac{4}{ab}\widetilde{\lambda}M\frac{\widetilde{u}(x_0,y_0)\sin\left(\frac{m\pi x_0}{a}\right)\sin\left(\frac{n\pi y_0}{b}\right)}{p_2\ \mathcal{C}_2(m,n)+p_1\mathcal{C}_1(m,n)-\widetilde{\lambda}\rho}, \tag{33}$$

for every $m,n \geq 1$. Evaluating (32) at $(x,y)=(x_0,y_0)$, using (33), we have

$$1 = \frac{4}{ab}\widetilde{\lambda}M\sum_{m,n=1}^{\infty}\frac{\sin^2\left(\frac{m\pi x_0}{a}\right)\sin^2\left(\frac{n\pi y_0}{b}\right)}{p_2\ \mathcal{C}_2(m,n)+p_1\mathcal{C}_1(m,n)-\widetilde{\lambda}\rho}, \tag{34}$$

which is the exact (series expression of the) frequency equation of the nanoplate with the point mass. The roots of (34) are the eigenvalues of the perturbed plate.

4. Perturbation analysis

Let us assume that the eigenvalues of the plate without point mass are simple. In this respect, it should be noticed that since we only need to consider the first three eigenfrequencies in our analysis, and the first eigenvalue is always simple, then this assumption is not particularly restrictive. We refer to [53] (Section 2.3) for a detailed analysis of the case of multiple eigenvalues in a simply supported plate in classical elasticity.

By general perturbation results, we know that the eigenpairs of the plate with the attached point mass M, with M small enough, depend analytically on the perturbation parameter M, i.e., there exists $\widehat{M}>0$ such that the eigenvalue as function of M, $\lambda=\lambda(M)$, is an holomorphic function of M for $0<M<\widehat{M}$. We shall derive an explicit expression of the first-order change of the eigenvalues with respect to M. Given a function f of the parameter M, we define the following forward-difference operator

$$\delta_h f(M) = \frac{f(M+h)-f(M)}{h}, \tag{35}$$

for every $h > 0$ and every $M > 0$. Let us recall the weak formulation (29) of the eigenvalue problem of the nanoplate with the point mass at $P_0 = (x_0, y_0)$ of magnitude $M + h$ and M, respectively:

$$\int_\Omega p_2 \Delta u(M+h)\Delta\varphi + p_1 \nabla(\Delta u(M+h)) \cdot \nabla(\Delta\varphi) = \\ = \lambda(M+h)\left((M+h)u(P_0; M+h)\varphi(P_0) + \int_\Omega \rho u(M+h)\varphi\right), \quad (36)$$

$$\int_\Omega p_2 \Delta u(M)\Delta\varphi + p_1 \nabla(\Delta u(M)) \cdot \nabla(\Delta\varphi) = \\ = \lambda(M)\left(M u(P_0; M)\varphi(P_0) + \int_\Omega \rho u(M)\varphi\right), \quad (37)$$

where, to simplify the notation, we have denoted by u, instead of $\widetilde{u}$, the eigenfunction of the perturbed problem and we have defined $u(x, y; M) = u(M)$, $u(x_0, y_0; M) = u(P_0; M)$. Note that, in the expressions above, φ is a function not depending on M.

Subtracting (37) to (36), and dividing by $\frac{1}{h}$, the left hand side (l.h.s.) becomes

l.h.s. of ((37)-(36))=

$$\int_\Omega p_2 \Delta(\delta_h u(M))\Delta\varphi + p_1 \nabla(\Delta(\delta_h u(M))) \cdot \nabla(\Delta\varphi), \quad \text{for every } \varphi \in \mathcal{H}, \quad (38)$$

whereas the right hand side (r.h.s.) is

r.h.s. of ((37)-(36))=

$$\frac{\lambda(M+h)}{h}\left((M+h)u(P_0; M+h)\varphi(P_0) + \int_\Omega \rho u(M+h)\varphi\right) - \\ - \frac{\lambda(M)}{h}\left(M u(P_0; M)\varphi(P_0) + \int_\Omega \rho u(M)\varphi\right), \quad \text{for every } \varphi \in \mathcal{H}. \quad (39)$$

It is convenient to add and subtract to (39) the quantity

$\frac{\lambda(M)}{h}\left((M+h)u(P_0; M+h)\varphi(P_0) + \int_\Omega \rho u(M+h)\varphi\right)$.

Further elaborating (39) we obtain

r.h.s. of ((37)-(36))=

$$\frac{\lambda(M+h)}{h}\left((M+h)u(P_0;M+h)\varphi(P_0)+\int_\Omega \rho u(M+h)\varphi\right)-$$
$$-\frac{\lambda(M)}{h}\left((M+h)u(P_0;M+h)\varphi(P_0)+\int_\Omega \rho u(M+h)\varphi\right)+$$
$$+\frac{\lambda(M)}{h}\left((M+h)u(P_0;M+h)\varphi(P_0)+\int_\Omega \rho u(M+h)\varphi\right)-$$
$$-\frac{\lambda(M)}{h}\left(Mu(P_0;M)\varphi(P_0)+\int_\Omega \rho u(M)\varphi\right)=$$
$$=\delta_h\lambda\left((M+h)u(P_0;M+h)\varphi(P_0)+\int_\Omega \rho u(M+h)\varphi\right)+$$
$$+\lambda(M)\left(\frac{(M+h)u(P_0;M+h)-Mu(P_0;M+h)+Mu(P_0;M+h)-u(P_0;M)}{h}\varphi(P_0)+\int_\Omega \rho(\delta_h u)\varphi\right)=$$
$$=\delta_h\lambda\left((M+h)u(P_0;M+h)\varphi(P_0)+\int_\Omega \rho u(M+h)\varphi\right)+$$
$$+\lambda(M)\left(u(P_0;M+h)\varphi(P_0)+M\delta_h u(P_0;M)\varphi(P_0)+\int_\Omega \rho(\delta_h u(M))\varphi\right). \quad (40)$$

By (38) and (40), we have

$$\int_\Omega p_2\Delta(\delta_h u(M))\Delta\varphi+p_1\nabla(\Delta(\delta_h u(M)))\cdot\nabla(\Delta\varphi)=$$
$$=\delta_h\lambda\left((M+h)u(P_0;M+h)\varphi(P_0)+\int_\Omega \rho u(M+h)\varphi\right)+$$
$$+\lambda(M)\left(u(P_0;M+h)\varphi(P_0)+M\delta_h u(P_0;M)\varphi(P_0)+\int_\Omega \rho(\delta_h u(M))\varphi\right), \quad (41)$$

for every $\varphi\in\mathcal{H}$. Now, we take $\varphi=u(M)$ and we notice that $\delta_h u(M)$ belongs to the admissible set of test functions $\mathcal{H}$ for the weak formulation of the eigenvalue problem (29). Then, the left hand side of (41) simplifies with the fourth and fifth terms of the r.h.s., and (41) becomes

$$0=\delta_h\lambda\left((M+h)u(P_0;M+h)u(P_0;M)+\int_\Omega \rho u(M+h)u(M)\right)+$$
$$+\lambda(M)u(P_0;M+h)u(P_0;M), \quad \text{for every } h>0. \quad (42)$$

Finally, letting $h\to 0^+$ and assuming continuity of the eigenfunctions with respect to the parameter h as $h\to 0^+$, we get

$$\frac{\partial\lambda(M)}{\partial M}|_{M^+}=-\lambda(M)\frac{u^2(P_0;M)}{Mu^2(P_0;M)+\int_\Omega u^2(M)}. \quad (43)$$

The left derivative is equal to the right derivative, and we have proved

$$\frac{\partial \lambda(M)}{\partial M}|_M = -\lambda(M)\frac{u^2(P_0;M)}{Mu^2(P_0;M)+\int_\Omega u^2(M)}. \tag{44}$$

From (44), we can conclude that the following Taylor's expansion holds true in a small neighborhood of the unperturbed plate (e.g., near $M = 0$)

$$\delta\lambda_n \equiv \widetilde{\lambda}_n - \lambda_n = -M\lambda_n u_n^2(P_0) + O(M^2), \tag{45}$$

for normalized unperturbed eigenfunction u_n, e.g., $\int_\Omega \rho u_n^2 = 1$. Note that, in (45), λ_n and $\widetilde{\lambda}_n$ denote the nth eigenvalue of the unperturbed and perturbed plate, respectively.

5. Identification of a point mass from minimal eigenfrequency data

Under the assumption of simple eigenvalues, let us introduce the quantities

$$S = \cos\left(\frac{2\pi x_0}{a}\right), \quad T = \cos\left(\frac{2\pi y_0}{b}\right), \tag{46}$$

where (x_0, y_0) is the position of the point mass of intensity M. Denote as

$$\delta\lambda_{11},\ \delta\lambda_{12},\ \delta\lambda_{21} \tag{47}$$

the first-order changes evaluated via (45), and let

$$C_{ij} = -\frac{\delta\lambda_{ij}}{\left(\frac{4}{\rho ab}\right)\lambda_{ij}}, \tag{48}$$

$(i, j) = (1, 1), (1, 2), (2, 1)$. Then, by adapting the arguments shown in [53], we have

$$T = \frac{C_{12}}{2C_{11}} - 1, \tag{49}$$

$$S = \frac{C_{21}}{2C_{11}} - 1, \tag{50}$$

$$M = \frac{4C_{11}}{(1-T)(1-S)}. \tag{51}$$

It should be noticed that the mass size M is uniquely determined, whereas, as expected by symmetry considerations, the position (x_0, y_0) is determined up to symmetric positions with respect to the axes $x = \frac{a}{2}$ and $y = \frac{b}{2}$. Let us also notice that the key point of the identification procedure is that the first eigenfunction u_{11} never vanishes inside Ω. This implies that the fundamental eigenvalue λ_{11} is always sensitive to the addition of the point mass, that is $C_{11} > 0$ for every position (x_0, y_0) of the point mass inside Ω.

6. Applications

6.1. The specimen

For the numerical calculations we consider a simply supported rectangular nanoplate with in-plane dimensions $a \times b$ and thickness h. The material properties are assumed as in [45]: $\gamma = 1000\ \frac{kg}{m^3}$, $E = 1.44\ GPa$, and $\nu = 0.38$. We also assume that the three scale parameters are equal [45], i.e., $\ell_0 = \ell_1 = \ell_2 = \ell = 17.6\ \mu m$. The dimensional analysis dictates that the eigenvalue $\widetilde{\lambda}_{mn}$ corresponding to bending vibration of the nanoplate with a point mass located in x_0, y_0 can be written as

$$\widetilde{\lambda}_{mn} = \frac{D}{\rho a^4}\widetilde{\Lambda}\left(m, n; \frac{x_0}{a}, \frac{y_0}{b}, \frac{a}{b}, \frac{\ell}{h}, \frac{a}{h}, \frac{M}{\rho ab}\right), \tag{52}$$

with $D = \frac{E}{1-\sigma^2}I$.

In the sequel we present results corresponding to $\frac{a}{b} = 0.8$, $\frac{a}{h} = 50$, and for several values of the dimensionless parameters $\frac{\ell}{h}$ and $\frac{M}{\rho ab}$.

6.2. Numerical perturbation analysis

Fig. 1 shows the difference between the first three eigenvalues $\widetilde{\lambda}_{11}, \widetilde{\lambda}_{12}, \widetilde{\lambda}_{21}$, calculated as roots of Eq. (34) (exact solution), and those obtained from the perturbative methodology using Eq. (45) neglecting the high order term $(\widetilde{\lambda}^*_{11}, \widetilde{\lambda}^*_{12}, \widetilde{\lambda}^*_{21})$. The difference has been calculated as $e_{mn} = \frac{\widetilde{\lambda}_{mn} - \widetilde{\lambda}^*_{mn}}{\widetilde{\lambda}_{mn}} \times 100$.

To solve (34), as it was done in previous works [54, 53], truncated series for $m = 6$ and $n = 5$ was considered. Numerical simulations have been carried out by dividing both sides of the plate into 50 equally sized intervals, for a total of 2500 nodes, and the mass M was alternatively located at all nodes of the mesh. The presented results correspond to $\frac{a}{h} = 50$, $\frac{\ell}{h} = 1$, and $\frac{M}{\rho ab} = \{0.005, 0.01\}$. The relative differences between exact eigenvalues and eigenvalues estimated via the perturbative solution have been represented by means of contour curves. In all the cases considered, the differences are very small and typically less than 0.25%. However, as it will be shown in the next section, discrepancies are large enough to introduce significant errors in the mass size when the point mass is located near the edges of the plate.

6.3. Identification results

In this section we present some results related to the identification methodology explained in section 5. For each mass position, the normalized spatial variables $u = \frac{x_0}{a}$, $v = \frac{y_0}{b}$ and the intensity of the mass M were evaluated using Eqs. (49)-(51) and Eq. (46) (note that the first eight eigenvalues of the plate are simple for the present case).

The mass was located in 2500 different points as explained in the previous section, and the percentage errors between the estimated and actual values were obtained for $\frac{a}{h} = 50$, three different mass sizes $\frac{M}{\rho ab} = \{0.0025, 0.0050, 0.0100\}$), and two values of the scale parameter $\frac{\ell}{h} = \{\frac{1}{10}, 1\}$. The results are summarized in Fig. 2 (mass size), Figs. 3 and 4 (position u and v, respectively). The percentage error in the estimation of the mass intensity was obtained as $e_M = \frac{(M_{est} - M)}{M} \times 100$, while the percentage errors for the position, e_u and e_v, were calculated as follows: $e_u = (u_{est} - u) \times 100$, and $e_v = (v_{est} - v) \times 100$ (note that (u, v) represents the normalized position of the mass with respect to the edges size, a and b, respectively). The maximum percentage error for M was obtained for $\frac{\ell}{h} = 1$, and it was equal to 15, 26, and 64 percent for $\frac{M}{\rho ab} =$

$\{0.0025, 0.0050, 0.0100\}$, respectively. Results have been obtained also for $\frac{\ell}{h} = \frac{1}{20}$ and $\frac{a}{h} = 75$, considering the same three values for the mass. The calculated percentage errors are similar to the previous cases, being the mass intensity the truly influential factor. The largest errors in mass identification were found for positions u, and v approximately belonging to the region $u + v \leq 0.5$.

Regarding the localization of the point mass, it is worth noting that the discrepancies on u and v are noticeably lower, and the maximum was found for $u < 0.20$ and $v < 0.20$.

7. Conclusions

The identification of added masses employing resonant based nanosensors is based on the fact that the eigenfrequencies have specific sensitivity to the added masses. The key issue is in extracting quantitative information on the mass intensity and its spatial distribution from a finite number of eigenfrequency data.

In this paper we analyze for the first time the bending vibration of a nanoplate with an attached mass using the strain gradient elasticity theory for homogeneous Lamé material, under Kirchhoff-Love's kinematical assumptions.

The direct problem is solved showing the effect of the attached mass in the natural frequencies of the nanoplate. The exact eigenvalues are obtained for a general case, and an approximate closed form expression is provided if the intensity of the mass is small.

The inverse problem of identifying an unknown point mass attached to a simply supported rectangular nanoplate from a minimal set of resonant frequency data has been also considered. For mass size small with respect to the total mass of the nanoplate, a perturbation approach based on an explicit expression of the eigenfrequency sensitivity to the point mass has been used to obtain closed-form expressions for the mass size and the two position variables in terms

of the first three resonant frequencies. Numerical results are in agreement with the theory and show that the mass size estimate is generally less accurate than the two position variables.

To the best of our knowledge, both the study of the direct free vibration problem and the inverse problem of determining the attached point mass from minimal eigenfrequency data have been addressed here for the first time.

The present contribution is a first step of a long-term research program aimed at the detection of more general mass distributions in nanoplates, such as mass per unit length concentrated along planar curves or mass per unit area assigned on two-dimensional subsets of the nanoplate. Significant work, both from the theoretical and experimental/numerical point of view, will be necessary to deal with this class of inverse problems, since, as it is well known, inverse eigenvalue problems with finite data pose challenging questions even in the more simple context of classical elasticity [55].

Acknowledgements

The authors from University Carlos III of Madrid wish to acknowledge *Ministerio de Economía y Competitividad de España* for the financial support, under grants number DPI2014-57989-P and DPI2013-45406-P. A. Morassi gratefully acknowledges the financial support of the National Research Project PRIN 2015$TTJN95$ *Identification and monitoring of complex structural systems.*

References

[1] I. Voiculescu, M. Zaghloul, Nanocantilever Beams: Modeling, Fabrication, and Applications, CRC Press, 2015.

[2] L. Teik-Cheng (Ed.), Nanosensors: theory and applications in industry, healthcare and defense, CRC Press, 2016.

[3] Q. Wang, B. Arash, A review on applications of carbon nanotubes and graphenes as nano-resonator sensors, Computational Materials Science 82 (2014) 350–360.

[4] G. Rius, F. Pérez-Múrano, Nanocantilever Beams: Modeling, Fabrication, and Applications, CRC Press, 2015, Ch. Nanocantilever beam fabrication for CMOS technology integration.

[5] M. Alvarez, L. Lechuga, Microcantilever-based platforms as biosensing tools, Analyst 135 (2010) 827–836.

[6] T. Braun, V. Barwich, M. Ghatkesar, A. Bredekamp, C. Gerber, M. Hegner, Micromechanical mass sensors for biomolecular detection in a physiological environment, Physical Review E 72 (2005) 031907.

[7] K. Gfeller, N. Nugaeva, M. Hegner, Micromechanical oscillators as rapid biosensor for the detection of active growth of escherichia coli, Biosensors and Bioelectronics 21 (2005) 528–533.

[8] N. Nugaeva, K. Gfeller, N. Backmann, H. Lang, M. Düggelin, M. Hegner, Micromechanical cantilever array sensors for selective fungal immobilization and fast growth detection, Biosensors and Bioelectronics 21 (2005) 849–856.

[9] R. Datar, S. Kim, S. Jeon, P. Hesketh, S. Manalis, A. Boisen, T. Thundat,

Cantilever sensors: nanomechanical tools for diagnostics, Mrs Bulletin 34 (2009) 449–454.

[10] K. Jensen, K. Kim, A. Zettl, An atomic-resolution nanomechanical mass sensor, Nature nanotechnology 3 (2008) 533–537.

[11] J. Chaste, A. Eichler, J. Moser, G. Ceballos, R. Rurali, A. Bachtold, A nanomechanical mass sensor with yoctogram resolution, Nature nanotechnology 7 (2012) 301–304.

[12] C. Ayela, L. Nicu, Micromachined piezoelectric membranes with high nominal quality factors in newtonian liquid media: a Lamb's model validation at the microscale, Sensors and Actuators B: chemical 123 (2007) 860–868.

[13] T. Xu, Z. Wang, J. Miao, L. Yu, C. Li, Micro-machined piezoelectric membrane-based immunosensor array, Biosensors and Bioelectronics 24 (2008) 638–643.

[14] X. Lu, Q. Guo, Z. Xu, W. Ren, Z. Cheng, Biosensor platform based on stress-improved piezoelectric membrane, Sensors and Actuators A: Physical 179 (2012) 32–38.

[15] T. Alava, F. Mathieu, L. Mazenq, C. Soyer, D. Remiens, L. Nicu, Silicon-based micromembranes with piezoelectric actuation and piezoresistive detection for sensing purposes in liquid media, Journal of Micromechanics and Microengineering 20 (2010) 075014.

[16] A. Bhaswara, H. Keum, S. Rhee, B. Legrand, F. Mathieu, S. Kim, L. Nicu, T. Leichle, Fabrication of nanoplate resonating structures via micro-masonry, Journal of Micromechanics and Microengineering 24 (2014) 115012.

[17] E. Kröner, On the physical reality of torque stresses in continuum mechanics, International Journal of Engineering Science 1 (1963) 261–278.

[18] R. A. Toupin, Elastic materials with couple-stresses, Archive for Rational Mechanics and Analysis 11 (1963) 385–414.

[19] R. A. Toupin, Theories of elasticity with couple-stress, Archive for Rational Mechanics and Analysis 17 (1964) 85–112.

[20] A. E. Green, R. S. Rivlin, Multipolar continuum mechanics, Archive for Rational Mechanics and Analysis 17 (1964) 113–147.

[21] R. D. Mindlin, Micro-structure in linear elasticity, Archive for Rational Mechanics and Analysis 16 (1964) 51–78.

[22] R. D. Mindlin, Second gradient of strain and surface-tension in linear elasticity, International Journal of Solids and Structures 1 (1965) 417–438.

[23] A. C. Eringen, Linear theory of nonlocal elasticity and dispersion of plane-waves, International Journal of Engineering Science 10 (1972) 233–248.

[24] A. C. Eringen, Nonlocal polar elastic continua, International Journal of Engineering Science 10 (1972) 1–16.

[25] A. C. Eringen, On differential-equations of nonlocal elasticity and solutions of screw dislocation and surface-waves, Journal of Applied Physics 54 (1983) 4703–4710.

[26] M. Eltaher, M. Khater, S. Emam, A review on nonlocal elastic models for bending, buckling, vibrations, and wave propagation of nanoscale beams, Applied Mathematical Modelling 40 (2016) 4109–4128.

[27] H. Rafii-Tabar, E. Ghavanloo, S. Fazelzadeh, Nonlocal continuum-based modeling of mechanical characteristics of nanoscopic structures, Physics Reports 638 (2016) 1–97.

[28] E. Benvenuti, A. Simone, One-dimensional nonlocal and gradient elasticity: closed-form solution and size effect, Mechanics Research Communications 48 (2013) 46–51.

[29] P. Lu, H. Lee, C. Lu, P. Zhang, Dynamic properties of flexural beams using a nonlocal elasticity model, Journal of Applied Physics 99 (2006) 073510.

[30] G. Romano, R. Barretta, M. Diaco, F. de Sciarra, Constitutive boundary conditions and paradoxes in nonlocal elastic nanobeams, International Journal of Mechanical Sciences 121 (2017) 151–156.

[31] N. Challamel, C. Wang, The small length scale effect for a non-local cantilever beam: a paradox solved, Nanotechnology 19 (2008) 345703.

[32] J. Fernández-Sáez, R. Zaera, J. Loya, J. Reddy, Bending of Euler-Bernoulli beams using Eringens integral formulation: a paradox resolved, International Journal of Engineering Science 99 (2016) 107–116.

[33] A. C. Eringen, Theory of nonlocal elasticity and some applications, Res Mechanica 21 (1987) 313–342.

[34] J. Fernández-Sáez, R. Zaera, Vibrations of Bernoulli-Euler beams using the two-phase nonlocal elasticity theory, International Journal of Engineering Science 119 (2017) 232–248.

[35] Z. B. Shen, H. L. Tang, D. K. Li, G. J. Tang, Vibration of single-layered graphene sheet-based nanomechanical sensor via nonlocal Kirchhoff plate theory, Computational Materials Science (2012) 200–205.

[36] T. Murmu, S. Adhikari, Nonlocal mass nanosensors based on vibrating monolayer graphene sheets, Sensors and Actuators B: Chemical 188 (2013) 1319–1327.

[37] S. M. Zhou, L. P. Sheng, Z. B. Shen, Transverse vibration of circular graphene sheet-based mass sensor via nonlocal Kirchhoff plate theory, Computational Materials Science (2014) 73–78.

[38] S. A. Fazelzadeh, E. Ghavanloo, Nanoscale mass sensing based on vibration of single-layered graphene sheet in thermal environments, Acta Mechanica Sinica 30 (2014) 84–91.

[39] D. Karličić, P. Kozić, S. Adhikari, M. Cajić, T. Murmu, M. Lazarević, Nonlocal mass-nanosensor model based on the damped vibration of single-layer graphene sheet influenced by in-plane magnetic field, International Journal of Mechanical Sciences 96 (2015) 132–142.

[40] S. Jalali, M. Naei, N. Pugno, A mixed approach for studying size effects and connecting interactions of planar nano structures as resonant mass sensors, Microsystem Technologies 21 (2015) 2375–2386.

[41] H. Askari, H. Jamshidifar, B. Fidan, High resolution mass identification using nonlinear vibrations of nanoplates, Measurement 101 (2017) 166–174.

[42] D. Lam, F. Yang, A. Chong, J. Wang, P. Tong, Experiments and theory in strain gradient elasticity, Journal of the Mechanics and Physics of Solids 51 (2003) 1477–1508.

[43] N. A. Fleck, J. W. Hutchinson, Strain gradient plasticity, Advances in Applied Mechanics 33 (1997) 295–361.

[44] P. Germain, The method of virtual power in continuum mechanics. Part 2: Microstructure, SIAM Journal on Applied Mathematics 25 (1973) 556–575.

[45] S. Kong, S. Zhou, Z. Nie, K. Wang, Static and dynamic analysis of micro beams based on strain gradient elasticity theory, International Journal of Engineering Science 47 (2009) 487–498.

[46] B. Wang, J. Zhao, S. Zhou, A micro scale Timoshenko beam model based on strain gradient elasticity theory, European Journal of Mechanics-A/Solids 29 (2010) 591–599.

[47] B. Wang, S. Zhou, J. Zhao, X. Chen, A size-dependent Kirchhoff microplate model based on strain gradient elasticity theory, European Journal of Mechanics-A/Solids 30 (2011) 517–524.

[48] B. Akgöz, Ö. Civalek, Strain gradient elasticity and modified couple stress models for buckling analysis of axially loaded micro-scaled beams, International Journal of Engineering Science 49 (2011) 1268–1280.

[49] B. Akgöz, Ö. Civalek, A new trigonometric beam model for buckling of strain gradient microbeams, International Journal of Mechanical Sciences 81 (2014) 88–94.

[50] L. Zhang, B. Liang, S. Zhou, B. Wang, Y. Xue, An application of a size-dependent model on microplate with elastic medium based on strain gradient elasticity theory, Meccanica 52 (2017) 251–262.

[51] A. Morassi, J. Fernández-Sáez, R. Zaera, J. Loya, Resonator-based detection in nanorods, Mechanical Systems and Signal Processing 93 (2017) 645–660.

[52] M. Dilena, M. Fedele Dell'Oste, J. Fernández-Sáez, A. Morassi, R. Zaera, Mass detection in nanobeams from bending resonant frequency shifts, Submitted (2017).

[53] L. Rubio, J. Fernández-Sáez, A. Morassi, Point mass identification in rectangular plates from minimal natural frequency data, Mechanical Systems and Signal Processing 80 (2016) 245–261.

[54] W. Ostachowicz, M. Krawczuk, M. Cartmell, The location of a concen-

trated mass on rectangular plates from measurements of natural vibrations, Computers an Structures 80 (2002) 1419–1428.

[55] D. Barnes, R. Knobel, The inverse eigenvalue problem with finite data for partial differential equations, SIAM Journal on Mathematical Analysis 26 (1995) 616–632.

Figure Captions

Figure 1. Differences in the three first eigenvalues $e_{mn} = \frac{\left(\widetilde{\lambda}_{mn} - \widetilde{\lambda}^{*}_{mn}\right)}{\widetilde{\lambda}_{mn}} \times 100$ for $\frac{M}{\rho a b} = 0.005$ and $\frac{M}{\rho a b} = 0.010$.

Figure 2. Error in the estimation of the point mass intensity, $e_M = \frac{(M_{est} - M)}{M} \times 100$, for two different values of the length scale parameter ($\frac{l}{h} = \frac{1}{10}$, $\frac{l}{h} = 1$), and three different values of the point mass ($\frac{M}{\rho a b} = 0.0025$, $\frac{M}{\rho a b} = 0.0050$, $\frac{M}{\rho a b} = 0.0100$).

Figure 3. Error in the estimation of the position u, $e_u = (u_{est} - u) \times 100$, for two different values of the length scale parameter ($\frac{l}{h} = \frac{1}{10}$, $\frac{l}{h} = 1$), and three different values of the point mass ($\frac{M}{\rho a b} = 0.0025$, $\frac{M}{\rho a b} = 0.0050$, $\frac{M}{\rho a b} = 0.0100$).

Figure 4. Error in the estimation of the position v, $e_v = (v_{est} - v) \times 100$, for two different values of the length scale parameter ($\frac{l}{h} = \frac{1}{10}$, $\frac{l}{h} = 1$), and three different values of the point mass ($\frac{M}{\rho a b} = 0.0025$, $\frac{M}{\rho a b} = 0.0050$, $\frac{M}{\rho a b} = 0.0100$).

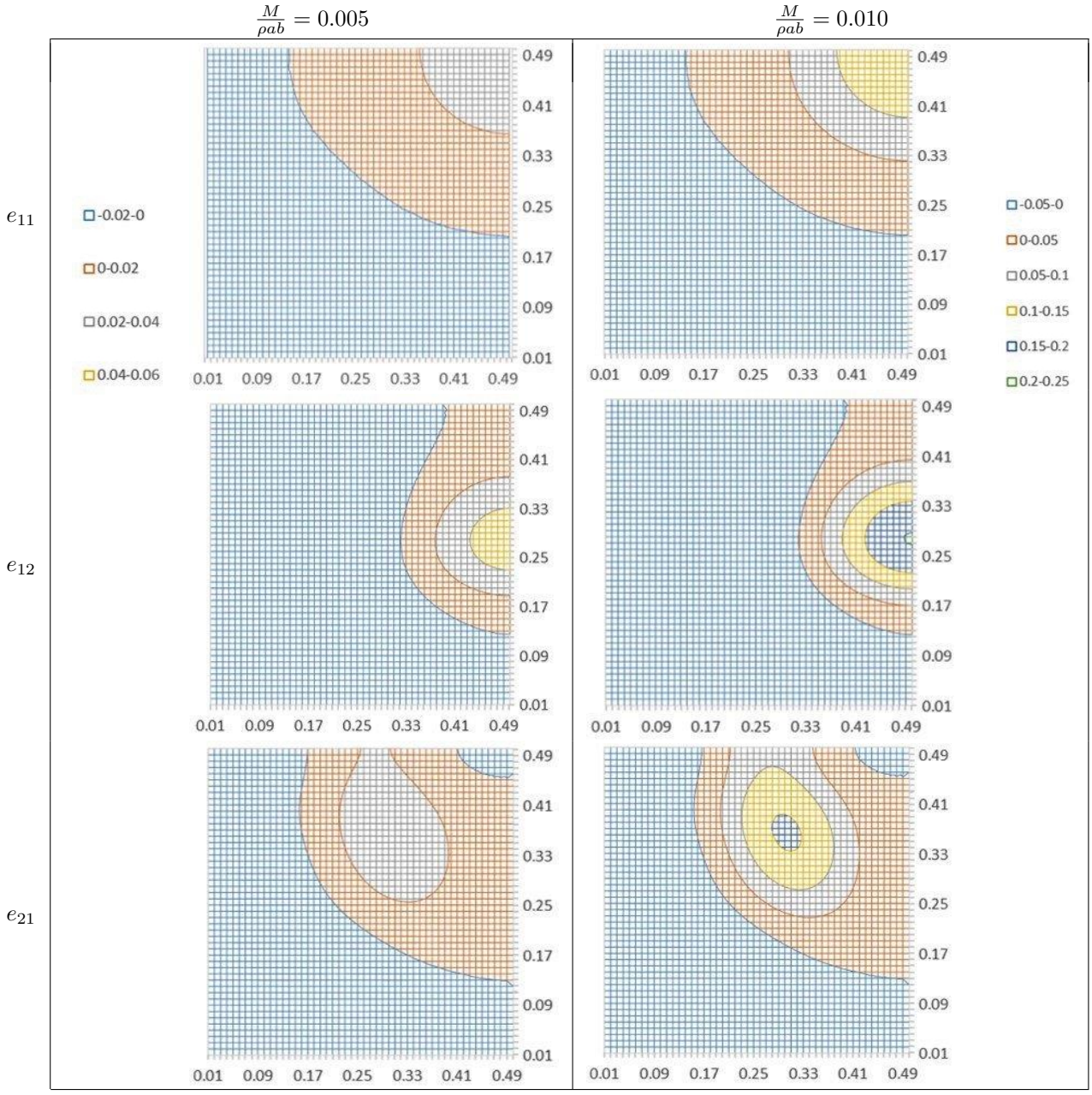

Figure 1: Differences in the three first eigenvalues $e_{mn} = \frac{(\tilde{\lambda}_{mn} - \tilde{\lambda}^*_{mn})}{\tilde{\lambda}_{mn}} \times 100$ for $\frac{M}{\rho ab} = 0.005$ and $\frac{M}{\rho ab} = 0.010$.

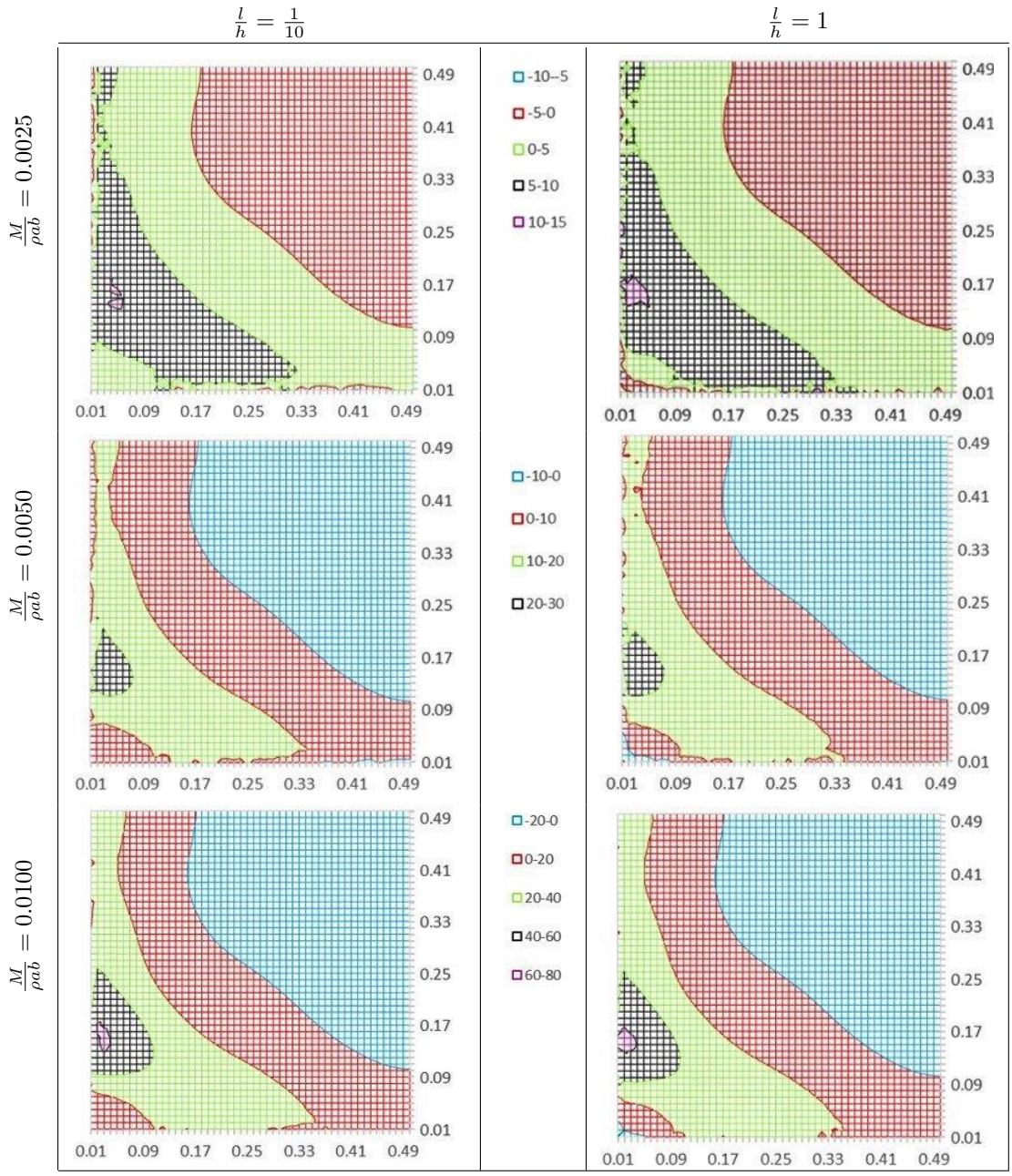

Figure 2: Error in the estimation of the point mass intensity, $e_M = \frac{(M_{est} - M)}{M} \times 100$, for two different values of the length scale parameter ($\frac{l}{h} = \frac{1}{10}$, $\frac{l}{h} = 1$), and three different values of the point mass ($\frac{M}{\rho ab} = 0.0025$, $\frac{M}{\rho ab} = 0.0050$, $\frac{M}{\rho ab} = 0.0100$).

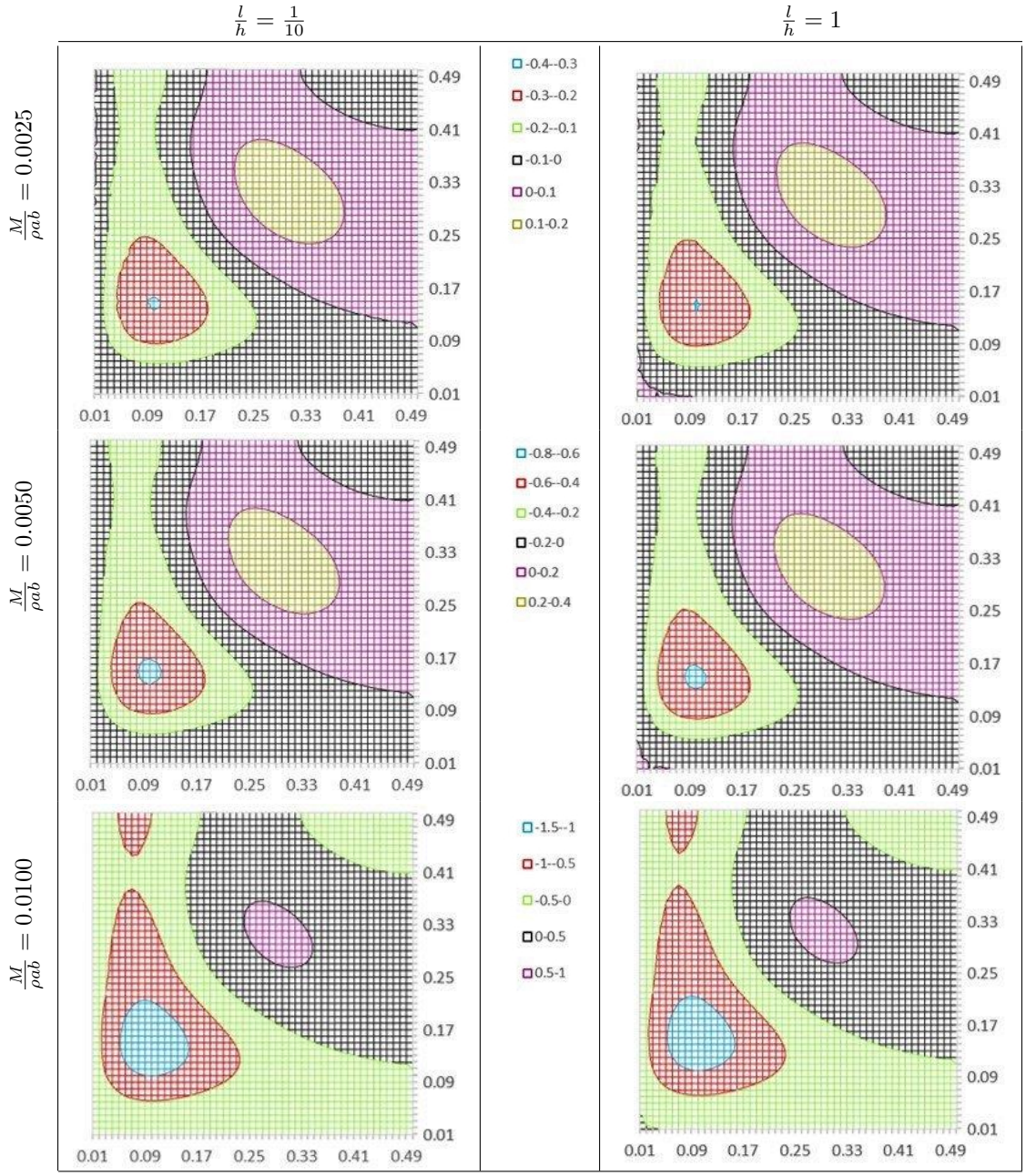

Figure 3: Error in the estimation of the position u, $e_u = (u_{est} - u) \times 100$, for two different values of the length scale parameter ($\frac{l}{h} = \frac{1}{10}$, $\frac{l}{h} = 1$), and three different values of the point mass ($\frac{M}{\rho ab} = 0.0025$, $\frac{M}{\rho ab} = 0.0050$, $\frac{M}{\rho ab} = 0.0100$).

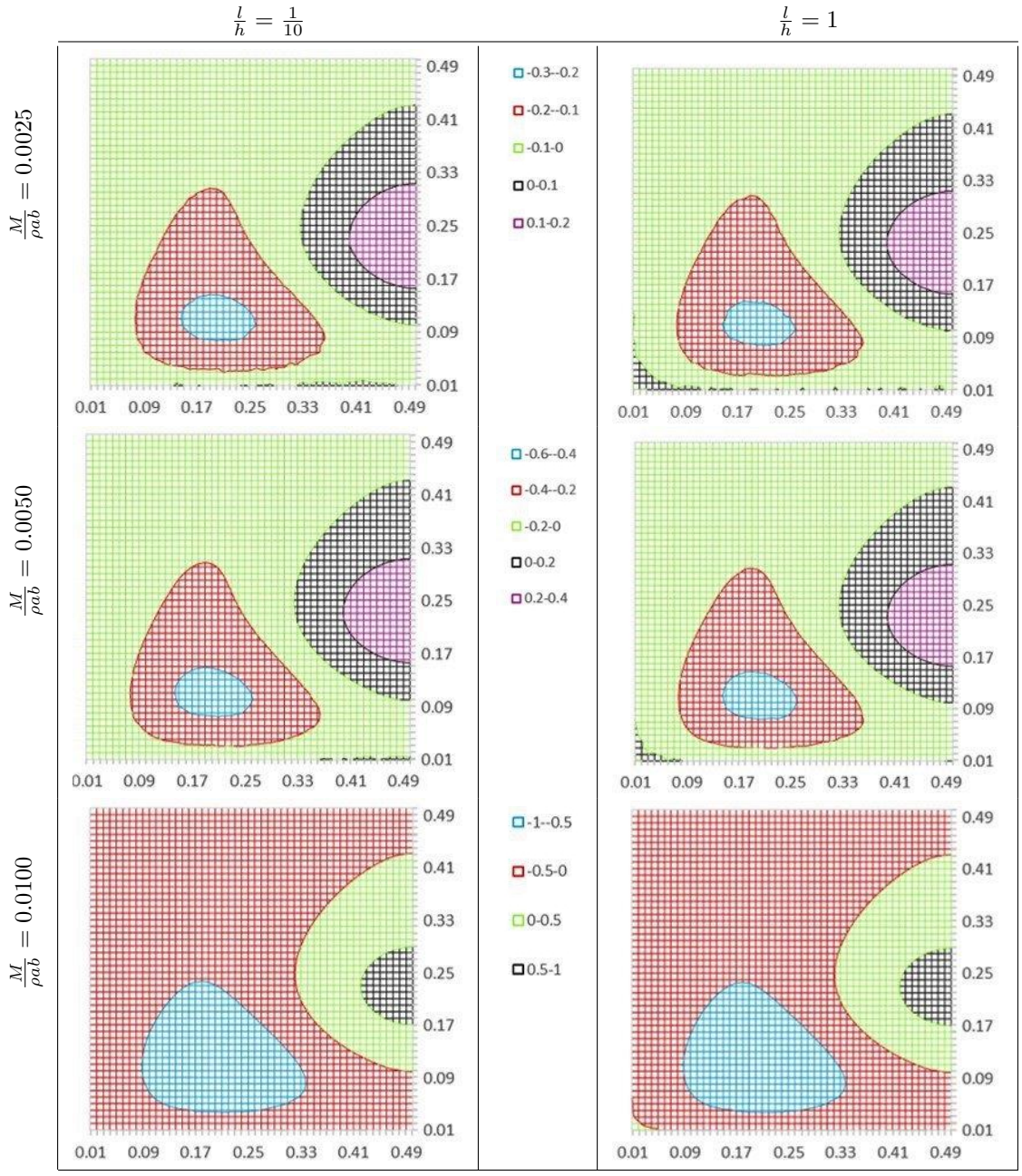

Figure 4: Error in the estimation of the position v, $e_v = (v_{est} - v) \times 100$, for two different values of the length scale parameter ($\frac{l}{h} = \frac{1}{10}$, $\frac{l}{h} = 1$), and three different values of the point mass ($\frac{M}{\rho ab} = 0.0025$, $\frac{M}{\rho ab} = 0.0050$, $\frac{M}{\rho ab} = 0.0100$).